AIP Journal of Applied Physics

Non-universal behavior well above the percolation threshold and thermal properties of core-shell-magnetite-polymer fibers

Sesha Vempati, Jagadeesh Babu Veluru, Raghuraman G. Karunakaran, Dhamodharan Raghavachari, and Natarajan T. Srinivasan

Citation: Journal of Applied Physics **110**, 113718 (2011); doi: 10.1063/1.3668890
View online: http://dx.doi.org/10.1063/1.3668890
View Table of Contents: http://scitation.aip.org/content/aip/journal/jap/110/11?ver=pdfcov
Published by the AIP Publishing

Non-universal behavior well above the percolation threshold and thermal properties of core-shell-magnetite-polymer fibers

Sesha Vempati,[1,a),b)] Jagadeesh Babu Veluru,[1,a),c)] Raghuraman G. Karunakaran,[2] Dhamodharan Raghavachari,[2] and Natarajan T. Srinivasan[1]
[1]*Department of Physics, Indian Institute of Technology Madras, Chennai 600 036, India*
[2]*Deparatment of Chemistry, Indian Institute of Technology Madras, Chennai 600 036, India*

(Received 16 August 2011; accepted 1 November 2011; published online 12 December 2011)

Aligned nanocomposite electrospun fibers are investigated for electrical (*dc*, *ac*, and dielectric) and thermal properties (10−40 wt.%). This nanocomposite consists of poly(methylmethacrylate) (PMMA) grafted core-shell magnetite (CSM) nanoparticles and PMMA. Electrical properties as a function of tunnel gap (in between the CSM nanoparticles) are studied as the polymer shell stays intact and the "cores" do not touch each other well above the percolation threshold. The depleted improvement in *dc* conductivity ($\sigma_{dcwt\%}$) with increasing wt.% (the improvement percentage: σ_{dc10} to $\sigma_{dc20} \approx 100\%$; σ_{dc20} to $\sigma_{dc30} \approx 40\%$ and σ_{dc30} to $\sigma_{dc40} \approx 1.2\%$) affirms the non-touching "cores" of CSM. Interestingly, the observed *ac* conductive behavior (0.1−13 MHz) in the high end of the frequency range is in clear contrast to that of a typical percolating system, in fact it does not explicitly follow the universal power law. Some of the obtained critical exponents are not accommodated by the universal theory and significantly different from the present theoretical/experimental predictions. Additionally, an improvement in thermal stability of ~30 °C and an overall increase in glass transition temperature are reported. © *2011 American Institute of Physics*. [doi:10.1063/1.3668890]

I. INTRODUCTION

The electrical conductivity and dielectric constant of metal/metal oxide and insulator percolation systems are widely investigated. These systems typically contain an insulating phase such as a polymer and a conducting phase such as carbon based materials,[1,2] metal, and metal salt.[3,4] Among these potential fillers, core-shell structures are of recent interest,[5] notably "magnetite." It is an important industrial material[6] that can be widely used in various applications[7,8] especially in biotechnology.[9] Such core-shell structured magnetite is a fascinating magnetic material capable of producing high magnetoresistance[10] when combined with some insulating barrier material. As previously mentioned, the electrical conductivity and dielectric constant of these composites are the most widely investigated properties; however, above the percolation limit, one can expect interesting features in *ac* conductivity and variation of the dielectric constant as a function of frequency. In this manuscript, such interesting features are explored. These nanocomposites (NCs) are potentially useful in electromagnetic interference (EMI) shielding[11,12] and bio-related fields.[13,14] Also, nanocomposite electrospun fibers (NCFs) prove to have considerable application potential.[15,16]

Most of the previous studies[2,17–19] have investigated the *ac* electrical conductivity (σ_{ac}) near and slightly above the percolation threshold. In these studies with reference to σ_{ac}, the frequency independent part is observed (also referred as *dc plateau*[20]) followed by frequency dependent part. We report, in contrast to previous studies, that the *dc* plateau is not observed at filling rates as high as ~8 times (10–40 wt.%) to the percolation threshold. Such high filling levels (well above percolation transition) are studied in literature, for example,[21] teflon and carbon (diameter $< 1\ \mu$m) mixtures with a percolation threshold of $\sim 0.290 \pm 0.005$. Further, a characteristic frequency is obtained, above which the critical exponent changes significantly, i.e., after the crossover frequency (*ac-ac* crossover), a new critical exponent is required to explain the conduction process in the entire frequency of present experimentation. Nevertheless, this data fit with presently accepted models and yield unusual critical exponents. Additionally, dielectric behavior as a function of frequency is studied and quantified via obtaining relevant critical exponents. Thermal properties are addressed in due course with regard to decomposition and glass transition temperature.

II. EXPERIMENTAL METHODS

Poly(methylmethacrylate) (PMMA) (Union Carbide, USA) and the solvent tetrahydrofuran (THF) (Sisco Research Laborites, India) were used as received. The synthesis of core-shell magnetite (CSM) nanoparticles and electrospinning is described elsewhere.[15,22] The process parameters are set as follows: (a) distance between the syringe-needle and the substrate was ~65 mm, (b) the diameter of the needle was 0.56 mm, (c) the rotating speed of collection screen was ~1500 rpm, (d) the solution flow rate ~0.65 μl/h. Initially, a known amount of CSM nanoparticles were dispersed in THF via sonication (ultrasonic agitation, 60 W) for 1 h. Required amount of PMMA was added to this dispersion in order to make 15 wt.% solution (optimized for electrospinning) in

[a)]Authors to whom correspondence should be addressed. Electronic addresses: bujjipavan@gmail.com and nnivjb@nus.edu.sg.
[b)]Present address: Center for nanostructured Media, School of Maths and Physics, Queen's University Belfast, BT7 1NN, United Kingdom.
[c)]Present address: Healthcare and Energy Materials Laboratory, National University of Singapore, Singapore 117 576, Singapore.

PMMA and 10, 20, 30, and 40 wt.% of CSM. These solutions were sonicated for 2 h and subjected to overhead stirring for 12 h. This well stirred solution was sonicated again for 1/2 h prior to electrospinning.

UV-visible spectra were recorded (Shanghai 756MC) from a dispersion of CSM, pure magnetite, and PMMA in THF. Electrospun fibers were imaged with JEOL JSM 840 A SEM from an Al foil. A drop of NCF's dispersion in hexane was collected on a holey carbon coated TEM grid and analyzed under JEOL JEM-2100 Electron Microscope. XRD patterns were obtained (X'Pert PRO PANalytical x-ray diffractometer, $\lambda = 1.5418$ Å) on pristine PMMA, electrospun PMMA fibers as well as on NCF-mat.

The fibers were collected (~1500 rpm) on a set of gold electrodes with a uniform separation of 1 mm for electrical characterizations. Later ~200 nm of gold is evaporated again with the same separation to ensure a reliable contact. Contact leads were obtained from these electrodes using a conducting silver dispersion. *dc* resistance was measured by employing Keithley 617 programmable electrometer and *ac* electrical properties were recorded with HP 4192 A Impedance Analyzer on the NCF-mat at room temperature (RT). The total cross-section of NCF-mat is obtained from the number of fibers and the average diameter (SEM images), henceforth the conductivity was calculated. Thermogravimetric analysis (TGA) was performed using Pyris 6, TGA (Perkin Elmer, USA), and differential scanning calorimetry (DSC) is carried out with Netzsch PC200 DSC on PMMA fibers and NCF-mat.

III. RESULTS AND DISCUSSION

A. Material characterization

UV-Vis spectra were recorded (Fig. 1) on Fe_3O_4, CSM and pristine PMMA to confirm the core-shell structure. In contrast to the largely silent feature in the visible region for magnetite nanoparticles, the CSM has shown clear bands at 270 and 320 nm corresponding to pure PMMA.[23] Inset in Fig. 1 shows a typical TEM image, depicting well dispersed CSM nanoparticles (see supplementary information for more TEM images (Fig. S1)[43]). The CSM nanoparticles have an aspect ratio close to 1.

It is known that the aspect ratio is one of the main concerns in determining the percolation threshold in *dc* electrical conductivity,[24] despite the fact that the absolute conductivity of the fillers does matter. Presently determined average diameter (~14 nm) and standard deviation (4 nm) are corroborated by an earlier report.[22]

Representative SEM images of NCF-mats are shown in Fig. 2 (see supplementary information, Fig. S2 for 20 wt.%). A close inspection of Fig. 2 reveals that 30 and 40 wt.% filling exhibited small clusters of CSM inside the fibers. Lower collection speed in fact results in unaligned/random fibers but definite improvement from 0 rpm. Inset in Fig. 2(c) shows the aligned fibers of 40 wt.% (~1500 rpm) which is significant indeed.[25] The average diameter of the fiber is ~3 μm with a standard deviation of ~1.1 μm (see supplementary information Fig. S3 for diameter distribution). However, obtaining fibers with uniform diameters is one of the challenges in electrospinning.[26]

TEM images of NCFs are shown in Fig. 3. The obtained images exhibit the distribution of CSM nanoparticles inside. No clusters of CSM nanoparticles are observed for 10 wt.%; however, small aggregations are observed in higher filling levels beyond 20 wt.%. Nevertheless, a significant amount of clustering occurred in 30 and 40 wt.%.

Fig. 4 depicts the XRD-patterns of pristine PMMA granuals, electrospun fiber-mat, and NCF-mat. The spectrum for granuals shows no significant peaks implying negligible crystallinity. In contrast, the pattern recorded for the PMMA fiber mat shows some peaks with a nominal intensity. Since the peaks are not well defined, the assignment to lattice indices cannot be done in this case. This proves again that the electrospinning in fact enhances the crystallinity of the polymers.[10,26–29] The NCF-mat depicted various peaks corresponding to magnetite. These peaks match with the

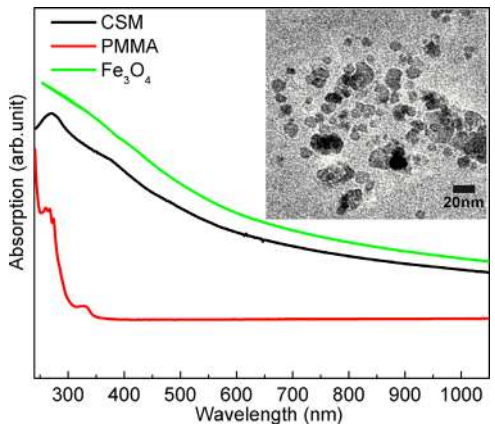

FIG. 1. (Color online) UV-Vis absorption spectra comparing Fe_3O_4 (magnetite) nanoparticles before and after grafting PMMA chains (i.e., CSM) compared with pristine PMMA. Inset shows TEM image of core-shell magnetite nanoparticles.

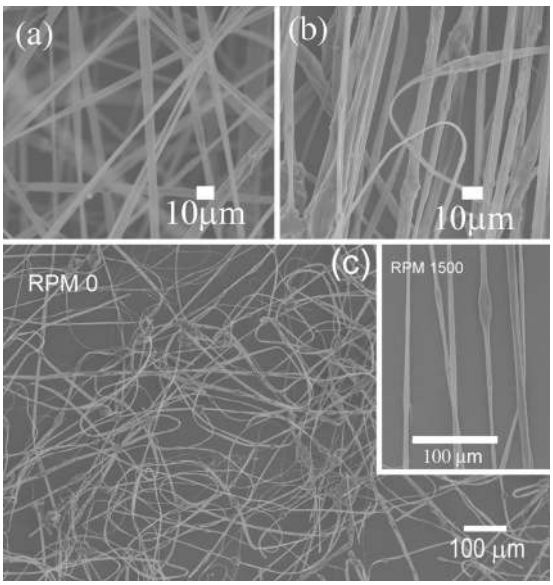

FIG. 2. SEM images of core-shell magnetite filled PMMA electrospun fibers: (a) 10 wt.% at ~800 rpm, (b) 30 wt.% at ~1200 rpm, (c) 40 wt.% at 0 rpm, inset at ~1500 rpm.

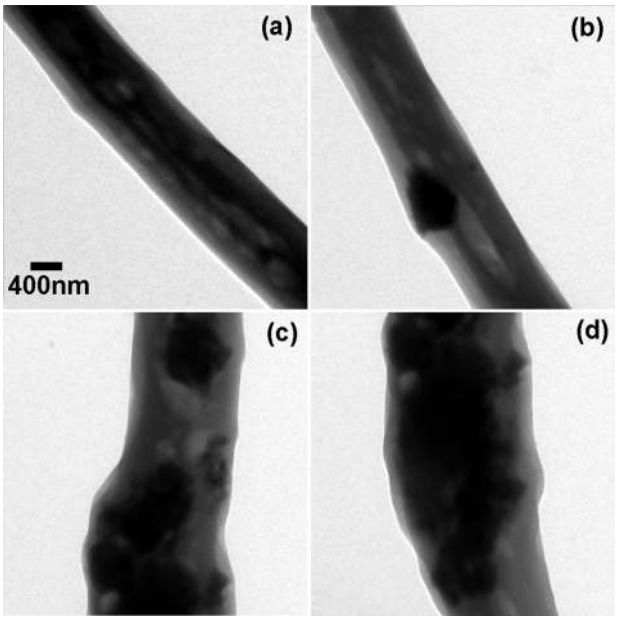

FIG. 3. TEM image of nanocomposite electrospun fibers of (a) 10, (b) 20, (c) 30, (d) 40 wt.% of core-shell magnetite loadings in PMMA.

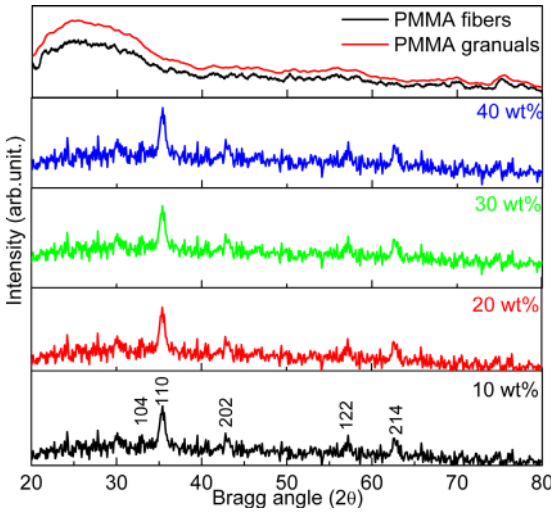

FIG. 4. (Color online) XRD patterns of pure PMMA granuals, PMMA-fiber mat, and nanocomposite fiber mat of filling levels 10-40 wt. %.

standard spectrum (JCPDS card No. 240081) and are annotated in Fig. 4.

Using Scherrer's equation, the mean crystallite diameter is calculated for NCF-mat and found to be $\sim 30 \pm 5$ nm, where the x-ray wavelength $= 1.5418$ Å and K is a shape factor $= 0.9$.[30]

B. Electrical properties

1. dc conductivity well above percolation

Electrical properties of a composite containing conductive fillers and insulating polymer are often analyzed in terms of the statistical percolation theory. At low concentration, conducting fillers are dispersed within the polymeric matrix as insulated clusters. Beyond a critical concentration (percolation threshold[31]), the conducting fillers connect to each other to form a network in the composite. Consequently, conductivity increases several orders of magnitude and also the dielectric properties are altered accordingly. Close to percolation threshold, the electrical properties have been investigated in various previous studies.[1,2,32] However, the present study reveals the electrical properties of the NCF at filling levels at least 2 to 5 times than the percolation threshold. In Fig. 5(a), *dc* conductivity of NCF is plotted as a function of CSM wt.% and the percolation transition (φ_c) is around 7–8 wt.%.

As the CSM wt.% is increased from 0 to 10, the σ_{dc} is increased by ~6 orders of magnitude from pristine PMMA.[33] The obtained σ_{dc} values are close to an earlier report[11] which deals with microwave hall mobility studies of same material. In our earlier report[10] on the core-shell structured Fe_3O_4 (referred to polymer grafted magnetite) of 5 wt.% filling, we measured $\sigma_{dc} \approx 12 \times 10^{-9}$ S/m (σ_{dc5}), so the values reported here represent an improvement of ~4 orders of magnitude. However, σ_{dc} is not improved with CSM wt.% as expected, i.e., $(\sigma_{dc20}-\sigma_{dc10})/\sigma_{dc10} \approx 100\%$, $(\sigma_{dc30}-\sigma_{dc20})/\sigma_{dc20} \approx 40\%$, $(\sigma_{dc40}-\sigma_{dc30})/\sigma_{dc30} \approx 1.2\%$, in contrast to $(\sigma_{dc10}-\sigma_{dc5})/\sigma_{dc5} \approx 2500\%$, which explicitly suggests some sort of saturation in the conductivity with filling level. Well above the φ_c, the conductivity improvement beyond 20 wt.% is not substantial due to the core-shell structure. As the concentration of the CSM is increased, the interparticle distance is decreased (see insets of Fig. 5(a) for various wt.% fillings) and an increase of σ_{dc} is observed.[20] This can be easily understood as at higher filling levels, the CSM nanoparticles are forming numerous conducting networks assisted by tunneling conduction. It is important to note that the nanoparticles are freely dispersed in the polymer matrix, in contrast to pelletized polymer composites.[1] To emphasize, in free dispersion there are slim chances that the cores of CSM touch/connect each

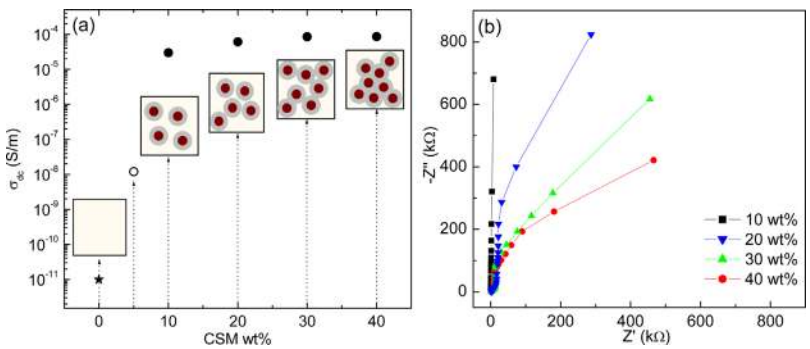

FIG. 5. (Color online) (a) Variation of *dc* conductivity (σ_{dc}) of nanocomposite fibers for various filling levels of core-shell magnetite at RT. (★) conductivity of pristine PMMA,[33] (○) *dc* conductivity for 5 wt.% of magnetite is obtained from literature.[10] Inset: grey box at 0wt.% indicates the pristine PMMA, density of magnetite nanoparticles are increasing with wt.%. (b) Nyquist plots for the nanocomposite fibers.

other in contrast to a pelletized composite. The determined[22] polymer chain-graft density (~5.7 chains/nm^2) disables the cores of CSM touching each other, which results in a rather high resistive path (high contact resistance) even while clustered. In spite of this, the improvement in the conductivity is a straight forward consequence of classical percolation theory with non-universal conduction mechanism, which considers the crucial influencing factors such as contact resistance and tunneling resistance.[34] Interparticle tunneling[35] causes the improvement in the conductivity of such composites, in which the conductive phase is lower than the φ_c. However, at the present level of filling ($>\varphi_c$), the conducting path is only assisted via tunneling/hopping. In Sec. III.B.2, it is explained that the hopping mechanism cannot support the observed *ac* conductivity. Hence, an immediate option is tunneling mechanism, which is the case with 5 wt.% CSM in PMMA (Ref. 10) and other filling levels as well.

2. ac conductivity

Well beyond the φ_c, *ac* dispersive behavior is investigated to reveal the ionic migration processes and also to find the appropriate critical exponents for the experimental data. It is evident from the TEM studies that CSM can be dispersed inside the host matrix even in very high filling levels, forming multiple CSM-CSM contacts that modify the electrical response of the composite. *ac* electrical behavior of these NCFs is investigated in the frequency regime 0.1–13 MHz (Fig. 5(b)–Fig. 7).

To start with, the Nyquist diagram is plotted in Fig. 5(b). Due to capacitive contribution one can remark the initial part of the semicircles/depressed semicircles for >20 wt.%. Nevertheless, the results are similar to those reported earlier for other polymer fibers.[4,36] It can be seen that the intercept of a typical curve on Z′ axis is high for lower concentration, i.e., lower filling level possesses higher *dc* resistance, which is in agreement with earlier *dc* conductivity measurements.

Moving on to *ac* conductivity (σ_{ac}), in all compositions, it is realized that there is no frequency independent conduction, which is generally attributed to resistive conduction through the NC (Fig. 6). However, to point-out a peculiar behavior, "*ac-ac*" crossovers or critical (characteristic) frequencies (ω_{01} and ω_{02}) are observed. ω_{01} and ω_{02} separates the three parts, namely (i), (ii), and (iii) (see Fig. 6(a) legend for various parts and see Table I for different ω_{01} and ω_{02}). Parts (i) and (ii) explicitly follow a power law behavior of the form $\sigma_{ac}(\omega) = \sigma_0 + a\omega^s$ in contrast to part (iii), where the conductivity starts to increase more rapidly, which is not clearly a classical power law. Here "*s*" is the critical exponent. It can be s_1 or s_2 depending on the region of interest (part (i)/(ii)), whereas the coefficient "*a*" is independent of temperature. Note that the $\sigma_0 = 0$ for all frequencies measured, i.e., there is no regime in which there is a frequency independent component of σ_{ac}. The obtained fitting parameters are tabulated in Table I. ω_{01} is chosen such that the error in both the least square fittings for parts (i) and (ii) is minimal in contrast to an earlier report[19] in which authors dealt with a "*dc plateau*" followed by a power law increase. It should be noted that ω_{01} and ω_{02} are almost invariant with CSM wt.%. Also, the exponent for the parts (i) and (ii) vary from 0.82 to 1.85. The unusual high exponent does not agree with the universality hypothesis[18] ($\sigma_{ac}(\omega) \propto \omega^s$, where $0.8 < s < 1$), which also indicates the non-dependency of the critical exponents on the details of cluster structures or interactions. As mentioned earlier, we investigate behavior in a regime 2 to 5 times higher than φ_c. At such high concentrations, it is expected that there are numerous network connections among the nanoparticles, in contrast to the regime which is close to φ_c. These numerous connections did not possess higher conductivity due to the intact polymer "shell" of nanoparticles. Hence, we suggest that the conduction can only be possible through the decrease in the tunneling distance between the particles.[17]

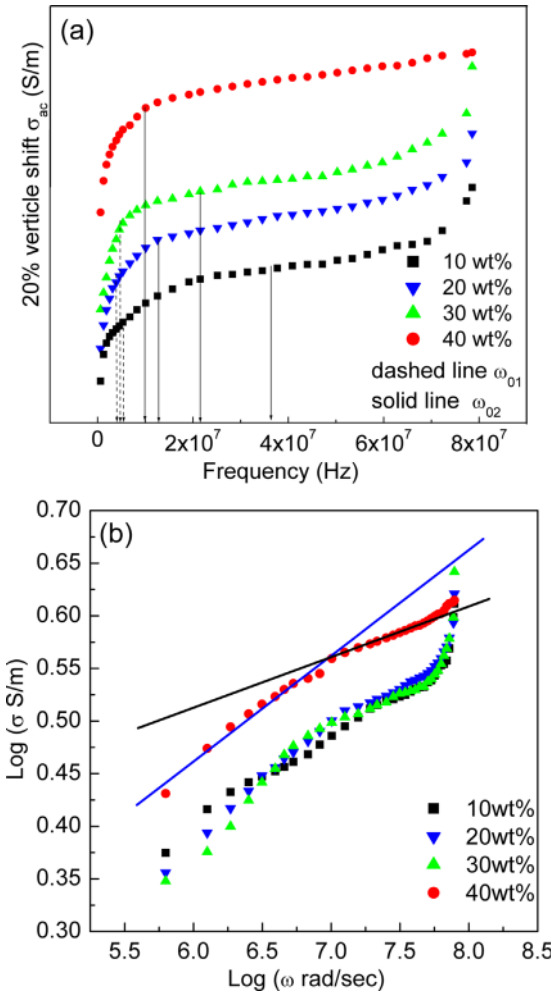

FIG. 6. (Color online) (a) *ac* conductivity (σ_{ac}, vertically shifted for clarity) of the nanocomposite fibers against frequency at RT. 0.1 MHz – ω_{01} Hz → part (i), ω_{01} – ω_{02} Hz → part (ii), and ω_{02} – 80 MHz → part (iii). (b) Log-log plot of *ac* conductivity versus frequency for the nanocomposite fibers of various filling levels.

Below, parts (i) and (ii) are individually addressed. Notably, part (iii) has not been observed in the literature previously, although the power law behavior in continuum percolation systems is previously well studied. Since the clusters are not fully percolating (due to the "shell" structure), and the apparent change in the *ac* conductivity must be due to a contribution from capacitance. At higher frequencies, the

TABLE I. Various critical exponents obtained from fittings are tabulated.

Wt. %	Part (i)$\sigma_{ac}(596\times10^3-\omega_{01})=a_1\omega^{s_1}$		Part (ii)$\sigma_{ac}(\omega_{01}-78.5\times10^6)=a_2\omega^{s_2}$		Loss tangent$tan\ \delta\propto\omega^{-z}$	
	$\omega_{01}\times10^6$(rad/s)	s_1	$\omega_{02}\times10^6$(rad/s)	s_2	$\omega_c\times10^6$(rad/s)	z
10	5.37	0.82 ± 0.01	25.12	1.26 ± 0.03	4	2.25 ± 0.03
20	3.89	1.85 ± 0.01	12.59	1.55 ± 0.03	4.5	3.56 ± 0.03
30	4.57	1.79 ± 0.03	21.38	0.85 ± 0.02	3.5	3.56 ± 0.02
40	NA	NA	10	1.24 ± 0.01	2	2.75 ± 0.03

capacitance contribution is rapidly increasing and hence part (iii) is noticed.

Part (i) can be explained by the power law of the form $\sigma_{ac}(596\times10^3-\omega_{01})=a_1\omega^{s_1}$. Linearly increasing conductivity (log-log scale) has occupied immense space in literature and is thoroughly explained. The power law exponent s_1 is expected to be between 0.8 and 1.0 for hopping mechanism,[37] which is the case with 10 wt.%. In contrast to this, higher fillings have depicted much higher s_1 values suggesting that the charge carriers do not follow the hopping mechanism. In this regime, σ_{ac} appears to be proportional (log-log scale) to frequency due to the capacitance of the host medium between the conducting particles or aggregates for all compositions. The increase in the σ_{ac} is attributed to the decrease in the tunneling distance between the fillers. Also the $\sigma_{ac(10\ to\ 30\ wt.\%)}$ are in the similar order with different s values, whereas σ_{ac40} has higher value. This similarity in σ_{ac} suggests that the decreased tunnel distance is not substantial till 30 wt.% to increase the *ac* conduction. However, in the context of σ_{dc}, the conduction is only assisted by tunneling of charge carriers, whereas σ_{ac} is supported by electronic as well as a contribution from ever decreasing impedance of capacitive part (see Fig. 5(b) and its discussion). In addition, the lower characteristic frequency, "ω_{01}" is not depicted by 40 wt.%, due to the saturated contact resistance.

Part (ii) can be described by power law ($\sigma_{ac}(\omega_{01}-78.5\times10^6)=a_2\omega^{s_2}$) with a different exponent (see Table I for s_2). Nevertheless, this linear dependency of the conductivity with frequency can be attributed to the electronic conduction with non-universal critical exponents.

In Part (iii), the sharp rise is explicitly observed for other samples except 40 wt.%. Rapid rise in the conductivity at high frequency attributed to the contribution from the capacitance. The Nyquist plot indicates a higher capacitance contribution in higher filling levels. In fact, all the samples possess some amount of capacitance contribution, but it is increasing with the CSM wt.%. The entire regime of conductivity is due to polarization (restricted moment) of permanent dipoles/induced dipoles/accumulated interfacial charges.

3. Dielectric characteristics

Figure 7(a) shows the frequency dependence of dielectric behavior of NCF at RT in the frequency range 0.1–13 MHz. Initially the capacitance was recorded and dielectric constant ($\varepsilon_r(\omega)$) was extracted using the following formula:[4] $\varepsilon_r(\omega)=[C(\omega)l]/\varepsilon_0 A$, where $C(\omega)$ is the frequency dependent capacitance, ε_0 is the free space dielectric constant, A is the total cross sectional area, and l is the distance between the electrodes. $\varepsilon_r(\omega)$ has shown weak frequency dependence from 0.1 to 1.8 MHz, after which it decreases rapidly.

This decrease can be attributed to the fact that in the higher frequencies, the heavier dipoles may not be able to align with the rapidly varying electric field.[4]

The dielectric constant is increasing with the filling rate in the entire frequency regime; however, a close overlap between 30 and 40 wt.% is observed in the high frequency end. Figure 7(a) inset is normalized capacitance (normalized individually, considering the maximum of each curve) versus frequency. The clustering/overlap of curves exhibit the similarity in the dielectric behavior, which is simply the scaling of universal behavior. Figure 7(b) depicts a plot between loss tangent (*tan* δ) and log frequency. The behavior is fitted

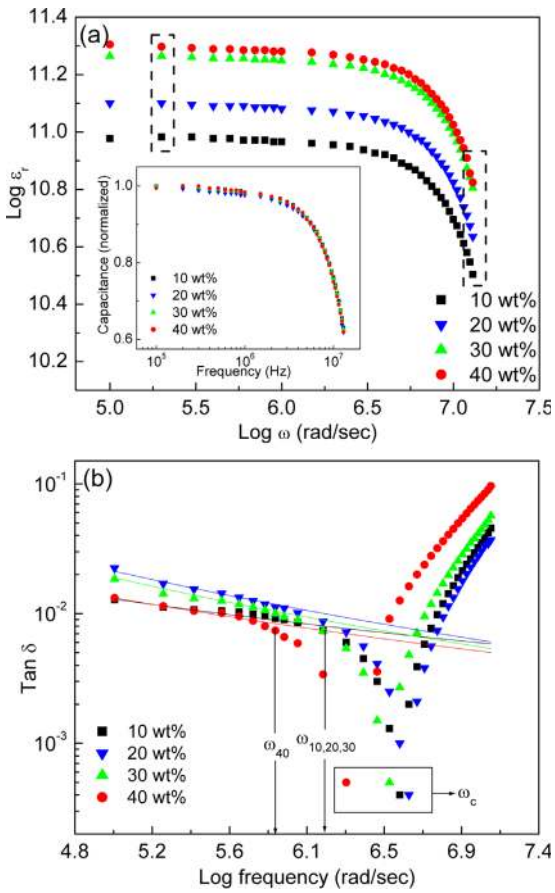

FIG. 7. (Color online) Dielectric properties of nanocomposite fibers. (a) Log-log plot of dielectric constant ($\varepsilon_r(\omega)$) versus frequency (rad/s). Inset is a plot of normalized (independently) capacitance versus frequency (Hz) on log scale, (b) variation of *tan* δ against frequency at RT. ω_c stands for critical frequency at which *tan* δ is the minimum.

to the following power-law equation $tan\ \delta \propto \omega^{-z}$ and the obtained parameters are tabulated in Table I. The fitting deviates from the data if the frequency is above $\omega_{10,20,30}$ ($\sim 9.3 \times 10^6$ rad/s) for 10–30 wt. % and ω_{40} ($\sim 5.6 \times 10^6$ rad/s) for 40 wt.%. After crossing a critical frequency ω_c (the minimum in *tan* δ) *tan* δ starts to increase more rapidly. In the case of 40 wt.%, the raise has appeared little earlier than the other concentrations (see Table I for ω_c). Behavior similar to this is observed in the literature in a Fe_3O_4 and polymer system,[1] in which the authors have noticed a minimum in *tan* δ. They have also noticed for a filling level below φ_c, *tan* δ is reasonably well frequency dependent, in agreement with intercluster polarization predictions. Further, the authors[1] found no explanation for the rise after ω_c, which is a small tail in their observation. In the present filling levels ($>\varphi_c$), the *tan* δ is less frequency dependent below ω_c. Nevertheless, here the rise in *tan* δ can be observed explicitly, and unfortunately no explanation has been found in literature.

C. Thermal properties

1. Thermal stability

The thermograms of pure PMMA fibers and the NCFs were plotted for comparison in Fig. 8(a). In the case of pure PMMA, only one degradation step between 360 to 370 °C can be observed, corresponding to a number of reactions leading to monomer units until the PMMA is volatilized completely.[38] The decomposition temperature (T_d) associated with this degradation step is affected by the presence of CSM. It is clear from the TGA graphs that the thermal stability of the NCF is increased when compared with pristine PMMA fibers, presumably due to the restriction of mobility of oxide particles. However, the increase is not varying much with the CSM wt.%, which suggests a saturation in thermal stability with filler content (see Fig. 8(b) inset). The increase in the thermal stability ~30 °C is indeed a significant result,[39] which may be attributed to the enhanced compatibility of filler with the host matrix[40,41] due to the surface modification of magnetite.

2. Glass transition

The glass transition temperature (T_g) was determined from the DSC profiles (Fig. 8(b)) by the location of the midpoint of the ΔC_p (the heat capacity change in the vicinity of T_g) function and the width assigned by the end points of the ΔC_p function, i.e., the T_g is estimated by the midpoint of the jump in heat capacity. The DSC profiles show an endothermic transition, starting at ~80 °C and centered at ~90 °C which indicates the evaporation of water molecules from the polymer matrix. In the region of 100 to 130 °C, there is no substantial deviation of the base line. Also the T_g is dependent on the molecular weight as well as the degree of crystallinity of the polymer. When the temperature crosses 140 °C, one can observe the exothermic regime, which may be because of crystallization of the polymer. Inset in Fig. 8(b) emphasizes that there is a slight overall improvement in the T_g, which is corroborated with XRD results depicting improved crystallinity.

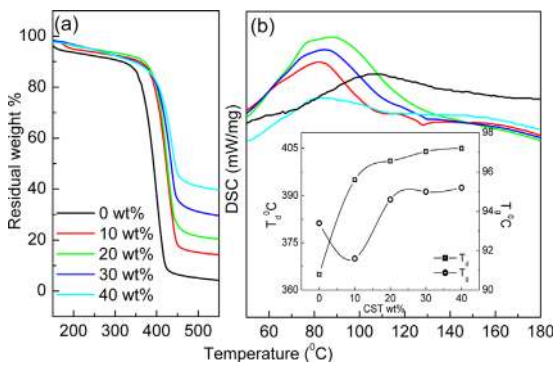

FIG. 8. (Color online) Thermal properties of pristine PMMA fibers and nanocomposite fibers. (a) TGA curves recorded under nitrogen atmosphere. (b) DSC profiles, inset shows decomposition and glass transition temperatures (T_d and T_g, respectively) for various filling levels. Connecting lines are only for the guidance to the eye.

The presence of CSM lowered the mobility of the chains, and as a result, the T_d and T_g increased for NCFs. In addition, the increase in the concentration of nanoparticles makes the nanocomposite more brittle, leaving even less "*free*" space for the polymer macromolecules to move.[42]

IV. SUMMARY AND CONCLUSIONS

The main aspect of this paper is to understand the electrical (*dc*, *ac*, and dielectric) properties in the nearly extreme limits of filling ratios, such as 40 wt.% where the cores of CSM nanoparticles do not touch each other. It is demonstrated that the electrospun fibers with improved crystallinity (corroborated with XRD and DSC) at higher loadings of magnetic fillers might possess unusual and interesting electrical characteristics, which may find potential applications in various fields. Such a nanocomposite could be employed as both high-dielectric constant material and conductive polymer.

Improvement in the *dc* conductivity with filling level is not as high as expected due to the polymer "shell" of the magnetite. In higher concentrations even if the adjacent particles are touching, the conduction might happen only through the tunneling between the particles which results in a high contact resistance. The enhanced conductivity of ~6 orders of magnitude with filling rate is due to the decreased tunneling distance as well as an increased number of tunneling pathways. Since the σ_{ac} did not follow universal phenomenon, a theoretical model is required to fully explain this peculiar conduction behavior. However, it is attempted to explain the perceived conduction behavior with the existing models. A least square fit is undertaken to the data with an equation of the following form $\sigma_{ac}(\omega) = a_1'\omega^{s_1'} + a_2'\omega^{s_2'}$ to realize the inherent dependency of the exponents. But curve fitting was not very successful indicating the non-dependency of the exponents. Dielectric response in fact followed the universal scaling behavior in contrast to σ_{ac} in which no scaling is observed.

It can be expected that further filling levels may also be dielectric in nature, rather than highly conductive, which may be a very significant finding. Further increase in the filling level (>40 wt.%) has lead to unsuccessful electrospinning. Study on thermal properties suggests an enhancement of 30 °C in decomposition temperature and slight improvement in the glass transition temperature due to improved compatibility of the filler.

ACKNOWLEDGMENTS

We wish to thank Indian Institute of Technology Madras and Council of Scientific and Industrial Research (CSIR) for financial support.

[1]C. Chiteme and D. S. McLachlan, Phys. Rev. B **67**, 024206 (2003).
[2]S. Barrau, P. Demont, A. Peigney, C. Laurent, and C. Lacabanne, Macromolecules **36**, 5187 (2003).
[3]Y.-J. Li, M. Xu, and J.-Q. Feng, Appl. Phys. Lett. **89**, 072902 (2006).
[4]V. J. Babu, V. S. P. Kumar, S. Bibekananda, V. R. K. Murthy, and T. S. Natarajan, Mater. Sci. Eng. B **142**, 46 (2007).
[5]F. Wang, X. Chen, Z. Zhao, S. Tang, X. Huang, C. Lin, C. Cai, and N. Zheng, J. Mater. Chem. **21**, 11244 (2011).
[6]Y. Shen, Y. Lin, and C.-W. Nan, Adv. Funct. Mater. **17**, 2405 (2007).
[7]D. Vollath, Adv. Mater. **22**, 4410 (2010).
[8]E. D. L. Cruz-Montoya and C. Rinaldi, J. Appl. Phys. **107**, 09B506 (2010).
[9]A. M. G. C. Diasa, A. Hussaina, A. S. Marcosa, and A. C. A. Roque, Biotechnol. Adv. **29**, 142 (2010).
[10]V. S. Pavan Kumar, V. Jagadeesh Babu, G. K. Raghuraman, R. Dhamodharan, and T. S. Natarajan, J. Appl. Phys. **101**, 114317 (2007).
[11]D. V. B. Murthy, V. Subramanian, V. S. P. Kumar, T. S. Natarajan, G. K. Raghuraman, R. Dhamodharan, and V. R. K. Murthy, J. Appl. Polym. Sci. **107**, 1967 (2008).
[12]K. Singh, A. Ohlan, A. K. Bakhshi, and S. K. Dhawan, Mater. Chem. Phys. **119**, 201 (2010).
[13]Q. Zhang, V. N. Mochalin, I. Neitzel, I. Y. Knoke, J. Han, C. A. Klug, J. G. Zhou, P. I. Lelkes, and Y. Gogotsi, Biomaterials **32**, 87 (2011).
[14]K.-Y. Chun, Y. Oh, J. Rho, J.-H. Ahn, Y.-J. Kim, H. R. Choi, and S. Baik, Nat. Nanotechnol. **5**, 853 (2010).
[15]B. Sundaray, V. Subramanian, T. S. Natarjan, R.-Z. Xiang, C.-C. Chang, and W.-S. Fann, Appl. Phys. Lett. **84**, 1222 (2004).
[16]A. Baji, Y.-W. Mai, S.-C. Wong, M. Abtahi, and X. Du, Compos. Sci. Technol. **70**, 1401 (2010).
[17]J. Wu and D. S. McLachlan, Phys. Rev. B **56**, 1236 (1997).
[18]J. C. Dyre and T. B. Schroder, Rev. Mod. Phys. **72**, 873 (2000).
[19]B. E. Kilbride, J. N. Coleman, J. Fraysse, P. Fournet, M. Cadek, A. Drury, S. Hutzler, S. Roth, and W. J. Blau, J. Appl. Phys. **92**, 4024 (2002).
[20]K.-M. Jager, D. H. McQueen, I. A. Tchmutin, N. G. Ryvkina, and M. Kluppel, J. Phys. D: Appl. Phys. **34**, 2699 (2001).
[21]Y. Song, T. W. Noh, S. I. Lee, and J. R. Gaines, Phys. Rev. B **33**, 904 (1986).
[22]G. K. Raghuraman and R. Dhamodharan, J. Nanosci. Nanotechnol. **6**, 2018 (2006).
[23]P. Liu and Z. Su, J. Macromol. Sci. Part B-Phys. **45**, 131 (2006).
[24]S. White, R. Mutiso, P. Vora, D. Jahnke, S. Hsu, J. M. Kikkawa, J. Li, J. E. Fischer, and K. I. Winey, Adv. Funct. Mater. **20**, 2709 (2010).
[25]C. A. Bashur, L. A. Dahlgren, and A. S. Goldstein, Biomaterials **27**, 5681 (2006).
[26]Z.-M. Huang, Y.-Z. Zhang, M. Kotakic, and S. Ramakrishna, Compos. Sci. Technol. **63**, 2223 (2003).
[27]X. M. Mo, C. Y. Xu, M. Kotaki, and S. Ramakrishna, Biomaterials **25**, 1883 (2004).
[28]K. H. Lee, H. Y. Kim, Y. M. La, D. R. Lee, and N. H. Sung, J. Polym. Sci., Part B: Polym. Phys. **40**, 2259 (2002).
[29]D. H. Reneker, W. Kataphinan, A. Theron, E. Zussman, and A. L. Yarin, Polymer **43**, 6785 (2002).
[30]U. Schertmann and R. M. Cornell, *Iron Oxides in the Laboratory: Preparation and Characterization* (VCH, Weinheim, 1991).
[31]C. W. Nan, Prog. Mater. Sci. **37**, 1 (1993).
[32]S. J. Chin, P. Hornsby, D. Vengust, D. Mihailovic, J. Mitra, P. Dawson, and T. McNally, "Composites of poly(e-caprolactone) and $Mo_6S_3I_6$ Nanowires," Polym. Adv. Technol. (2010).
[33]D. Charles, R. C. Weast, and S. M. Selby, *Handbook of Chemistry and Physics* (Chemical Rubber Company, Cleveland, OH, 1960).
[34]X. Sun and M. Song, Macromol. Theory Simul. **18**, 155 (2009).
[35]W. Wang, M. Yu, Y. Chen, and J. Tang, J. Appl. Phys. **99**, 08J108 (2006).
[36]J. B. Veluru, K. K. Satheesh, D.C. Trivedi, M. V. Ramakrishna, and N. T. Srinivasan, J. Eng. Fibers Fabrics **2**, 25 (2007).
[37]V. Rao, P. Ashokan, and M. Shridhar, Mater. Sci. Eng., A **281**, 213 (2000).
[38]D. Lopez, I. Cendoya, F. Torres, J. Tejada, and C. Mijangos, Polym. Eng. Sci. **41**, 1845 (2001).
[39]D. Sun, N. Miyatake, and H. J. Sue, Nanotechnology **18**, 215606 (2007).
[40]E. Bourgeat-Lami, P. Espiard, A. Guyot, C. Gauthier, L. David, and G. Vigier, Angew. Makromol. Chem. **242**, 105 (1996).
[41]S. Hayashi, Y. Takeuchi, M. Eguchi, T. Iida, and N. Tsubokawa, J. Appl. Polym. Sci. **71**, 1491 (1999).
[42]P. Dallas, V. Georgakilas, D. Niarchos, P. Komninou, T. Kehagias, and D. Petridis, Nanotechnology **17**, 2046 (2006).
[43]See supplementary material at http://dx.doi.org/10.1063/1.3668890 for additional transmission electron micrograms of CSM, scanning electron microgram of 20 wt.% fibers and diameter distribution of the electrospun fibers.